Electrochimica Acta 507 (2024) 145085

Contents lists available at ScienceDirect

Electrochimica Acta

journal homepage: www.journals.elsevier.com/electrochimica-acta

Using the nonlinearity of a PEM water electrolyzer cell for its dynamic model characterization

Pietari Puranen [a,*], Michael Hehemann [b], Phillip Kütemeier [b], Lauri Järvinen [a], Vesa Ruuskanen [a], Antti Kosonen [a], Jero Ahola [a], Pertti Kauranen [a]

[a] Lappeenranta–Lahti University of Technology LUT, P.O. Box 20, FI-53851, Lappeenranta, Finland
[b] Forschungszentrum Jülich GmbH, Wilhelm-Johnen-Straße, DE-52428, Jülich, Germany

ARTICLE INFO

Keywords:
Green hydrogen
Water electrolysis
Dynamic modeling
Equivalent circuit

ABSTRACT

The voltage response of a water electrolyzer at low frequencies is characterized by a combination of a static polarization curve and dynamic, capacitive effects. In this paper, a model combining these two phenomena is created, which incorporates the Butler–Volmer equation in parallel with a capacitance in order to produce differential equations for the activation overpotentials separately on both electrodes. A parameter fitting methodology is then developed for obtaining the seven model parameters from a set of low-frequency, high-amplitude dynamic waveform measurements. The method is further implemented in an electrolyzer modeling toolbox for MATLAB. The model built in this study is proven to predict well both static and dynamic voltage responses down to the 1 Hz frequency. At higher frequencies and at small amplitudes the model reduces to the Randles equivalent circuit, and in a static case to the polarization curve of the cell. The proposed methodology can be used for probing individual electrode properties with full-cell measurements and providing a reliable tool for simulating water electrolyzer voltage responses with arbitrary waveforms and amplitudes.

1. Introduction

According to Faraday's law of electrolysis, hydrogen production from electrochemical water splitting is directly proportional to the current supplied to the cell. As a result, water electrolyzers are ideally supplied with uniform DC current. This ideal condition is, however, not always met. The voltage response, and thus power consumption, of the cell also depend on the dynamic changes of input current, its amplitude and frequency. In grid-connected industrial water electrolyzer systems, the commonly used thyristor-based power electronic rectifiers induce a significant AC ripple on top of the DC current they supply, which has been found to increase the power consumption of water electrolyzers [1]. Operation at partial loads further increases the significance of the ripple. Moreover, with electrolyzers being increasingly controlled by the energy generation of renewable sources, the load level of the electrolyzer will be more variable, which means that the dynamic performance of cells and stacks will play an even greater role in the future. Frequency ranges of these two sources of dynamic power differ, renewable energy sources mostly causing low-frequency variation roughly below 1 Hz due to changing weather conditions and seasons [2] and power electronics producing AC ripple above 300 Hz [3]. To fully explore these phenomena and control their effect, it is essential to have system models capable of taking into account both static and dynamic performance regardless of the AC frequency or amplitude.

Electrochemical impedance spectroscopy (EIS) is a commonly used dynamic cell characterization method, which is based on the assumed linearity of the voltage response at low amplitudes. The modeling of EIS results is generally based on equivalent circuit models with linear electronic components, such as resistors and capacitors, but also nonlinear components like the constant phase element, which describes the behavior of porous electrodes [4]. All of the equivalent circuits are linear, and as such, their impedance is well determined and easily calculable. The applicability range of these equivalent circuits can be somewhat extended by recognizing that at the higher frequency range of ripple produced by power electronics, the voltage response of water electrolyzers is approximately linear regardless of the current AC amplitude [5]. At lower frequencies, however, the static polarization curve adds a nonlinear effect to the large-amplitude voltage response. The significance of this nonlinearity increases as the frequency is reduced, converging eventually to the static behavior of the polarization curve. Example current density–voltage representations of the nonlinear static polarization curve, the linear response to an EIS measurement and the nonlinear large-amplitude dynamic response of a single water electrolyzer cell are given in Figs. 1(a), 1(b) and 1(c), respectively.

* Corresponding author.
E-mail address: pietari.puranen@lut.fi (P. Puranen).

https://doi.org/10.1016/j.electacta.2024.145085
Received 19 April 2024; Received in revised form 9 September 2024; Accepted 17 September 2024
Available online 21 September 2024

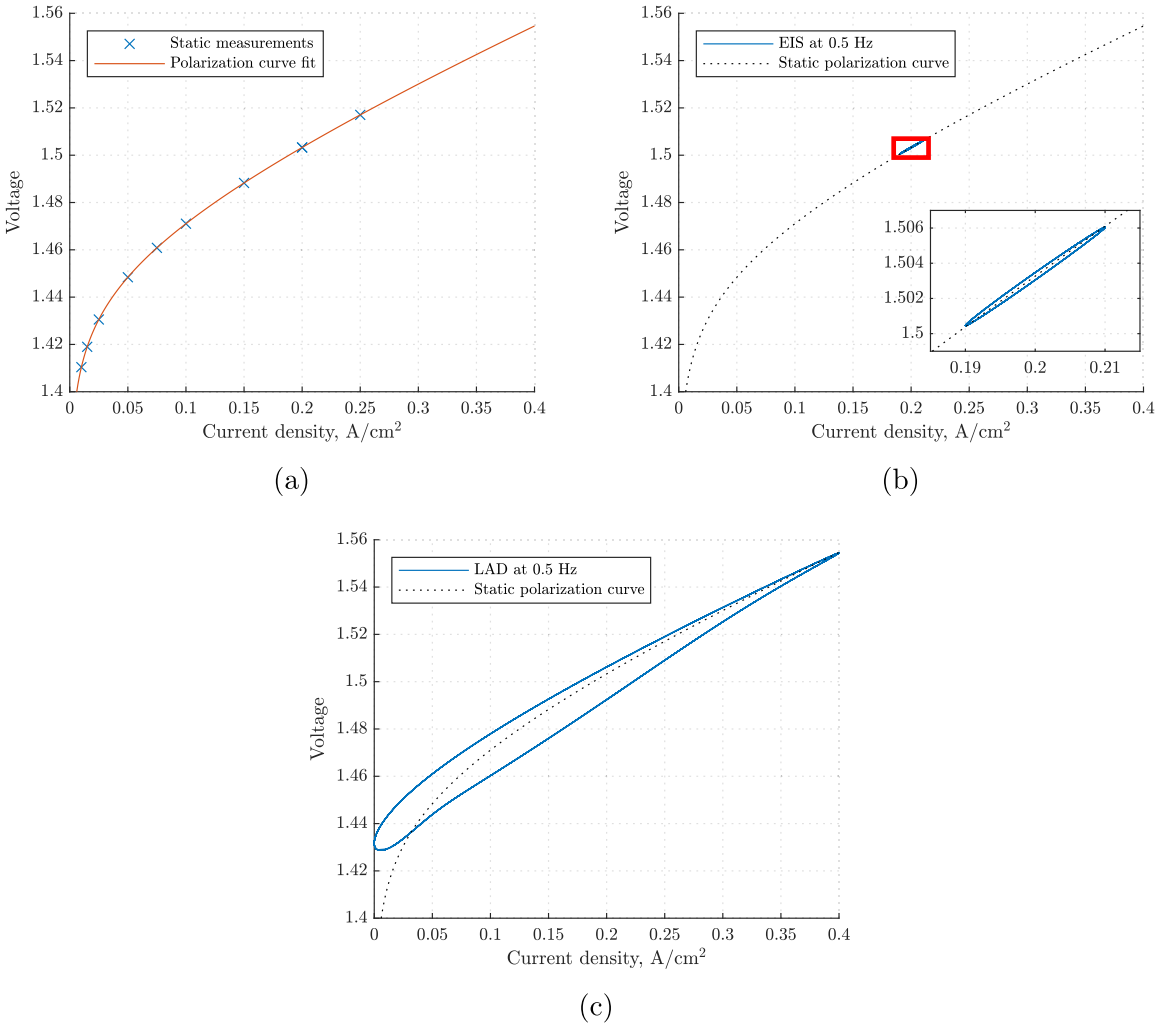

Fig. 1. Example current–voltage representations of (a) the nonlinear static polarization curve of a water electrolyzer cell, (b) a linear response for an EIS measurement at 0.5 Hz and (c) a large-amplitude dynamic (abbreviated for the figure as LAD) response at 0.5 Hz. All three figures have been simulated using the model created and parametrized in this paper.

Both the linear equivalent circuit modeling and the nonlinear static polarization curve modeling are well established in the literature. The nonlinear transition between these two modes of operation is, however, less studied. Closer inspection on this frequency range can provide novel characterization and analysis tools for water electrolyzer research.

Multiple studies have used linear equivalent models of various complexities for water electrolyzer dynamics. In particular, these methods have been proven useful in reproducing step responses [6,7]. Either the studied step responses [7] or EIS [8,9] can be used for the model parametrization. One issue with the linear equivalent circuits is, however, that they cannot take into account the static response. By separating the nonlinear static and linear dynamic parts, Amireh et al. [10] were able to bypass this issue. Nevertheless, the linearity of the dynamic model limits its usage to either small AC amplitudes or high frequencies, where the voltage response approaches linear [5].

Some ways of representing the nonlinear dynamics have been presented in the literature. Ursua and Sanchis [11] introduced an equivalent circuit model with current-dependent activation resistances. Their model has to be parametrized by using a large set of polarization curve and EIS measurements in different setpoints. Zenith et al. [12] approached the issue with a set of analytic and differential equations for calculating a time constant for a high-temperature polymer fuel cell. A similar differential-equation-based solution was proposed by Immerz et al. [13] to analyze over- and undershoot phenomena in PEM water electrolyzers under galvanostatically and potentiostatically controlled stepwise load changes. Krenz et al. [14] solved the differential equation after a current interruption and used this solution with experimental results for parametrizing an industrial PEM water electrolyzer. Their model simplified the system to a single electrode with one kinetic-induced time constant.

Beyond simply modeling the electrochemical systems, their nonlinear behavior has been utilized in various characterization methods. Fasmin and Srinivasan [15] reviewed methods aiming to expand the applicability of EIS to large amplitudes, the nonlinear EIS (NLEIS) methods, also interchangeably called nonlinear frequency response analysis (NFRA). The methods are based on applying a large-amplitude sinusoidal signal and analyzing the response in the frequency domain concentrating on either only the fundamental frequency as a function of applied amplitude or separately on each frequency component. Vidaković-Koch et al. [16] performed another review on the topic, differentiating between NLEIS and NFRA, the former concentrating on the changes in the fundamental frequency and the latter also comprising the harmonic components. The methodology of NFRA is often based on series expansions of the response, which are then compared with suitable models. Wolff et al. [17] analyzed theoretically the responses observable in the nonlinear harmonics of a general electrochemical system after changes in the system parameters. Their study presents a group of ways in which NFRA could be useful in analyzing a real system. In general, NFRA have mostly been used to investigate reaction

mechanisms and kinetics of specific technologies, for example PEM fuel cells [18,19], direct methanol fuel cells [20], and lithium-ion batteries [21,22].

In this paper, a method is presented for parametrizing a dynamic water electrolyzer model by using a simple fit to a set of voltage responses to sinusoidal, large-amplitude current excitations in time domain. The frequency range for the excitations is selected appropriately to especially allow capturing the transition from the high-frequency, impedance-based voltage response to the quasi-static, low-frequency response [5]. The model used in the study incorporates Butler–Volmer reaction kinetics separately for both the electrodes, with double-layer capacitances in parallel, as previously described by Immerz et al. [13]. The resulting model is solved numerically and as such allows arbitrary current waveforms to be used. The model and the fitting algorithm are incorporated into the Electrolyzer Modeling Toolbox for MATLAB by Järvinen and Puranen [23] to utilize its existing code base and methodology. A renewed version of the toolbox will be published after the required documentation and usage examples have been created.

The model and parametrization methodology presented in this paper enable characterizing PEM water electrolyzer electrodes separately by only using full-cell measurements. Compared with EIS, the model adds the inherent nonlinearity of the activation overpotential and expands the range of applicability to large-amplitude signals and low frequencies. However, the required measurements differ from EIS only by their amplitude and by the need for waveform measurements. As the signal frequencies are low, there is no fundamental need for the high sampling frequencies used in this paper. The experimental methodology is, therefore, accessible to laboratories of different levels, or it can be implemented in future designs of electrochemical measurement devices.

2. Theory

Water electrolysis is an electrochemical process where water molecules are split to hydrogen and oxygen with the aid of electricity following the overall reaction equation:

$$\mathrm{H_2O} \rightleftharpoons \frac{1}{2}\,\mathrm{O_2} + \mathrm{H_2}. \tag{1}$$

The process is split in two half-cell reactions: the anodic oxygen evolution reaction (OER) and the cathodic hydrogen evolution reaction (HER). The two electrodes are separated by a separator preventing direct electric contact but allowing ionic conduction. Electric connection between the two electrodes is obtained through a power supply.

In electrolysis, the power supply generates a potential difference between the electrodes which initiates the half-cell reactions. OER releases electrons which are transferred through the power supply to be bound by HER. The ions produced in the process, either cations or anions depending on the chosen technology, are transferred through the separator of the cell. The number of charge transfers needed for a single water splitting reaction is two.

The static voltage response of a water electrolyzer is commonly modeled by separating the total cell voltage to the reversible or open circuit potential (U_{ocv}), representing the minimum voltage required for the reaction to take place, and a set of current-dependent overpotentials, namely ohmic (U_{ohm}), activation (U_{act}), and concentration (U_{con}) overpotentials:

$$U = U_{\mathrm{ocv}} + U_{\mathrm{ohm}} + U_{\mathrm{act}} + U_{\mathrm{con}}. \tag{2}$$

Often, there is only a need to model the static behavior of the cell, but when the current input to the electrolyzer fluctuates, the voltage response has some slowness caused by internal capacitances in the cell. Dynamic modeling takes into account this capacitive behavior, and it can be used to analyze those characteristics of the cell that static models typically neglect. Additional power consumption caused, for example, by an alternating current input, has to be modeled dynamically [5].

2.1. Static modeling

Static modeling of the current–voltage behavior of electrolyzers rotates around the reversible open-circuit potential alongside irreversible overpotentials. In this study, the static modeling is based on well-known conventions summarized in detail for example by Järvinen et al. [24]. The open-circuit potential reflects the minimum voltage required to initiate the electrochemical reaction. This potential is considered constant if the environmental variables, temperature and pressure, stay unchanged. Its value can be calculated from environmental parameters by using the Nernst equation:

$$U_{\mathrm{ocv}} = U^\circ + \frac{\mathcal{R}T}{n_{\mathrm{e}}F}\ln\frac{\big(p_{\mathrm{cat}} - p_{\mathrm{sv}}(T)\big)\big(p_{\mathrm{an}} - p_{\mathrm{sv}}(T)\big)^{1/2}}{p^{\circ\,3/2}}, \tag{3}$$

where the standard potential U° is calculated by using an equation by Schalenbach [25]:

$$U^\circ = \frac{1}{n_{\mathrm{e}}F}\left[\big(-159.6\,\mathrm{J/(mol\,K)}\big)T + 2.8472\cdot 10^5\,\mathrm{J/mol}\right]. \tag{4}$$

The latter, pressure correction term in Eq. (3) takes into account the system pressure, where the cathode and anode absolute pressures are denoted by p_{cat} and p_{an}, respectively, and p° is a reference pressure of 1 bar. $p_{\mathrm{sv}}(T)$ is the saturation vapor pressure of pure water, which is calculated by an experimental equation presented by Balej [26]:

$$\log_{10} p_{\mathrm{sv}}(T) = 35.4462 - \frac{3343.93}{T} - 10.9\log_{10} T + 4.1645\cdot 10^{-3}T. \tag{5}$$

The constants in Eq. (3) are the Faraday constant, F, the universal gas constant, $\mathcal{R}$, and the number of electrons required for a single electrochemical reaction, n_{e}, which is 2 in the case of water electrolysis (described by Eq. (1)).

Overpotentials cause an irreversible energy loss in the system, with causes ranging from simple resistive losses for transferring charges to the requirements of overcoming the activation barrier of the reaction. All overpotentials increase as a function of the current density j through the cell.

Ohmic overpotential is used to describe the voltage increase caused by resistive losses in the system. Its modeling is simply based on Ohm's law:

$$U_{\mathrm{ohm}} = rj, \tag{6}$$

where r represents the area-specific resistivity of the whole system.

Losses inflicted by the reaction kinetics are represented by the activation overpotential, commonly implicitly expressed by the Butler–Volmer equation:

$$j = j_0\left[\exp\left(\frac{\alpha n_{\mathrm{e}}F}{\mathcal{R}T}U_{\mathrm{act}}\right) - \exp\left(-\frac{(1-\alpha)n_{\mathrm{e}}F}{\mathcal{R}T}U_{\mathrm{act}}\right)\right], \tag{7}$$

where j_0 is the exchange current density, and α is the electron transfer coefficient, both being temperature-dependent properties of the specific cell [27]. An additional independent variable in the equation is the temperature T. Because of the implicit nature of the Butler–Volmer equation, a number of approximations have been introduced for solving the activation overpotential, for example, the Tafel equation:

$$U_{\mathrm{act}} = \frac{\mathcal{R}T}{\alpha n_{\mathrm{e}}F}\ln\frac{j}{j_0}, \tag{8}$$

and the hyperbolic sine approximation:

$$U_{\mathrm{act}} = \frac{\mathcal{R}T}{\alpha n_{\mathrm{e}}F}\operatorname{arsinh}\frac{j}{2j_0}. \tag{9}$$

The different approximations and their range of validity are discussed in more detail, for example, by Järvinen et al. [24].

Concentration overpotential is inflicted by a build-up of product gases on the reaction site [28]. This leads to bubbles shielding the electrode surface, which, in turn, reduces the utilization of the catalyst. As a result, the potential of the reaction increases. Generally, the current density has to be high for the concentration overpotential to be significant. As the current density is limited to be low in this study, the concentration overpotential cannot be distinguished, and thus, has to be omitted in the models.

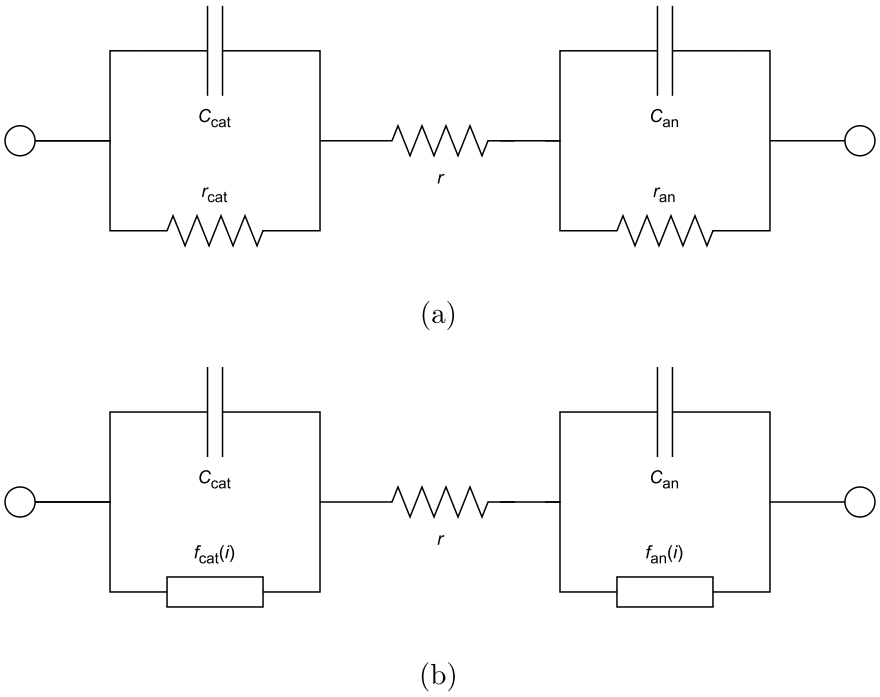

Fig. 2. (a) Linear Randles equivalent circuit for small-signal modeling and (b) its modified version replacing activation resistances with the Butler–Volmer equation.

2.2. Dynamic modeling

Dynamic modeling of electrolyzer cells comes in question when the current through the cell is not constant over time. In dynamic operation, the static polarization curve is not sufficient for describing the current–voltage behavior but also capacitive effects in the cell have to be considered.

A commonly employed dynamic analysis method is the electrochemical impedance spectroscopy (EIS), which is based on including a sinusoidal small-signal perturbation on top of the desired DC current or voltage. Using a small amplitude with the perturbation, usually below 5% of the applied DC value, allows omission of the nonlinearity caused by reaction kinetics (activation overpotential). The response can, thus, be approximated to be linear, enabling the calculation of a complex impedance for the system. The frequency of the perturbation is then varied to obtain a frequency spectrum of impedances. A variety of linear equivalent circuit models have been developed to replicate the EIS spectra consisting of simple electrical components, like resistors, capacitors, and inductors, but also more complicated ones, like the constant phase element (CPE) [9].

The part that differentiates dynamic equivalent circuits from the static model, described in Section 2.1, is the handling of activation overpotentials. Activation overpotentials arise from the kinetics of the reactions occurring at the boundary layer between the electrode and the electrolyte, the electrochemical double layer (EDL) [29]. In dynamic modeling, capacitive effects arising from these layers of ions have also to be taken into account [30]. As the capacitance does not prevent a DC current flow through the double layer, it is modeled in parallel with the activation overpotential.

The simplest equivalent circuit used for modeling EIS spectra is the Randles equivalent circuit, shown in Fig. 2(a). The Randles circuit approximates the activation overpotential with a simple resistor, causing the circuit to be linear. This approximation limits the use of the circuit, as well as other linear equivalent circuits, to small perturbations only, such as the ones used in EIS. Linearization enables the use of simple equations for fitting EIS results, or alternatively, allows increasing the complexity of the circuit. Linear circuits cannot reproduce the nonlinear behavior of the activation overpotential observed at high amplitudes and low frequencies, which limits their usability.

To create a large-signal model for water electrolysis, the nonlinearities of the activation overpotential have to be included. The concept presented in this paper (Fig. 2(b)) is based on the Randles equivalent circuit, but replacing the activation resistances with the full Butler–Volmer equation, Eq. (7). To do this, we have to look at the current density j flowing through the parallel connection of a capacitor and the Butler–Volmer equation:

$$j(t) = j_{\mathrm{act}}(t) + j_{\mathrm{C}}(t), \tag{10}$$

where j_{act} and j_{C} are the current densities through the activation and the capacitor, respectively. When connected in parallel, the voltage across both the branches is equal, U_{act}. The current through the capacitor depends on the time derivative of voltage:

$$j_{\mathrm{C}}(t) = C\frac{\mathrm{d}U_{\mathrm{act}}(t)}{\mathrm{d}t}, \tag{11}$$

where C is the capacitance density. Eq. (7) is used for the activation current, denoted here only by j_{act} for simplicity. Substituting it and Eqs. (11) to (10), a differential equation is obtained for the activation overpotential:

$$\frac{\mathrm{d}U_{\mathrm{act}}(t)}{\mathrm{d}t} + \frac{1}{C}\left(j_{\mathrm{act}}\left(U_{\mathrm{act}}(t)\right) - j(t)\right) = 0, \tag{12}$$

which has the measured current density as an excitation term. The same equation has to be applied twice, separately for both electrodes.

The full dynamic model for the cell is obtained by combining Eqs. (3), (4), (6), (12), and (7) to (2) (assuming no concentration overpotential) to achieve a set of algebraic and differential equations:

$$U(t) = U_{\mathrm{ocv}} + U_{\mathrm{ohm}} + U_{\mathrm{act,cat}}(t) + U_{\mathrm{act,an}}(t) \tag{2}$$

$$U_{\mathrm{ocv}} = U^{\circ} + \frac{\mathcal{R}T}{n_{\mathrm{e}}F}\ln\left[\frac{(p_{\mathrm{cat}} - p_{\mathrm{sv}}(T))(p_{\mathrm{an}} - p_{\mathrm{sv}}(T))^{1/2}}{p^{\circ 3/2}}\right] \tag{3}$$

$$U^{\circ} = \frac{1}{n_{\mathrm{e}}F}\left[(-159.6\,\mathrm{J/(mol\,K)})T + 2.8472\cdot 10^{5}\,\mathrm{J/mol}\right] \tag{4}$$

$$U_{\mathrm{ohm}} = rj \tag{6}$$

$$\frac{\mathrm{d}U_{\mathrm{act,x}}(t)}{\mathrm{d}t} = -\frac{1}{C_x}\left(j_{\mathrm{act},x}\left(U_{\mathrm{act,x}}(t)\right) - j(t)\right) \tag{12}$$

Table 1
Properties of the PEM cell used for the experiments.

Active area	17.64 cm^2
Membrane	Nafion™117
Cathode catalyst	Pt 0.39 mg/cm^2
Cathode PTL[a]	Toray paper
Anode catalyst	Ir 2.19 mg/cm^2
Anode PTL[a]	Sintered titanium coated with iridium

[a] PTL = Porous Transport Layer

$$j_{\mathrm{act},x}\left(U_{\mathrm{act},x}(t)\right) = j_{0,x}\left[\exp\left(\frac{\alpha_x n_{\mathrm{e},x} F}{\mathcal{R}T} U_{\mathrm{act},x}(t)\right) - \exp\left(-\frac{(1-\alpha_x) n_{\mathrm{e},x} F}{\mathcal{R}T} U_{\mathrm{act},x}(t)\right)\right], \quad (7)$$

where x denotes either the anode or the cathode (shortened an and cat, respectively). The number of electrons for a single reaction used in Eq. (7), $n_{\mathrm{e},x}$, is 2 in the case of cathode and 4 in the case of anode.

3. Methodology

3.1. Experimental methodology

The experimental measurements were conducted using a single-cell PEM test rig manufactured by FuelCon and located in Forschungszentrum Jülich (FZJ). The exact same setup was used previously by Koponen et al. [3] and Puranen et al. [5]. The system temperature was controlled at the cell inlet to match the given setpoint. Water heaters were located behind the separator vessels as well as around the cell inlet pipes and in the end plates of the cells, and system temperatures were measured using thermocouples. The water flow rates to the electrodes were controlled manually following measurements performed with two rotameters, one for each electrode. The pressure of the system was controlled with a set of two bubbling flasks creating a water column pressurizing the outlet. No actual pressure measurement or control was applied. The uncontrolled pressure makes it impossible to determine the exact value of the reversible potential. However, as also the exchange current density affects the potential in modeling just as if it was a voltage offset, any divergence of the reversible potential is included in the fit value of the exchange current density. As a result, both of these values have to be treated with caution. In this paper, the general behavior of the model is not affected by this uncertainty, which is why its significance for proving the functionality of the model is low.

The PEM water electrolyzer test cell used in the study was built in-house at FZJ. Its main properties are described in Table 1. A potentiostat (BioLogic HCP-1005) was used as the power source and waveform generator for this study. Current and voltage waveforms were recorded with an HBM Genesis HighSpeed GEN2tB transient recorder using a GN611B input card from the same company capable of up to a 200 kHz sampling frequency. The current measurement was performed with a Danisense DS200UB-10V current transducer with a maximum range of 200 A and a conversion factor of 1 V/20 A.

Measurements were performed in this study with the galvanostatic EIS functionality of the potentiostat. Unlike in conventional EIS measurements, where nonlinearities are avoided by using a low current amplitude, here the aim was to record the change in the nonlinearity as a function of frequency. Therefore, the DC setpoint was set to be reasonably low, 0.2 A/cm^2, to maximize the effect of the nonlinear activation overpotential, and the amplitude setpoint was assigned to 100% of DC. The frequency range between 1 Hz and 7.96 Hz was selected as it is known from previous research that the nonlinearity starts to have an effect on the specific cell in the chosen frequency range [5]. Further, the temperature of 80 °C was chosen. Current and voltage waveforms were recorded with sampling frequencies of 200 kHz with more than enough bandwidth for measuring harmonics.

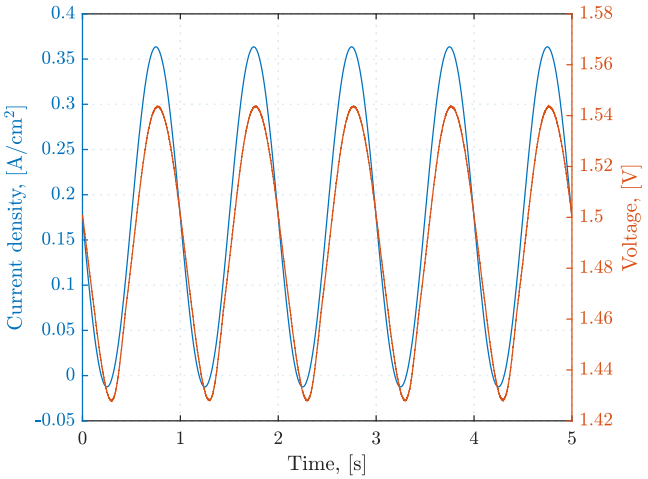

Fig. 3. Example of the measured waveforms at the frequency of 1 Hz.

3.2. Numerical methodology

The dynamic voltage response was modeled by using a modified version of the Electrolyzer Modeling Toolbox for MATLAB [23], where a new dynamic activation overpotential model incorporating Eq. (12) was added as one alternative. The basic functionality of the toolbox is described in [24]. The modifications included methodology for calculating the result based on a given current waveform and time data as well as performing a parameter fit to a dataset that includes current and voltage waveforms and their time signatures. An example of the current and voltage waveforms used for fitting is presented in Fig. 3 for a single frequency. The input data for fitting have to be provided in multiple frequencies for the procedure to reach a desired outcome.

Calculation of the full voltage response was performed in parts, separating the static submodels (reversible potential and ohmic overpotential, Eqs. (3) and (6), respectively) from the dynamic ones (activation overpotential, Eq. (12)). In this way, it is possible to reduce the complexity of the dynamic model. Static submodels can be algebraically solved by inputting the current waveform, environmental parameters, and constants, but a separate algorithm is required for solving the dynamic model.

Solving the differential equations of the dynamic model requires initial values of the separate activation overpotentials for the anode and the cathode. Because they could not be directly determined from the measured full-cell voltage, an optimization algorithm was developed with the aim of minimizing the time required for evaluating them. Differential equations themselves were solved by using the MATLAB ODE solver ode89 [31] capable of solving nonstiff differential equations in the form $y' = f(t, y)$.

After solving all static and dynamic submodels, their results were combined to the total cell voltage according to Eq. (2). The fitting procedure was then based on minimizing the square root of the sum of squared residuals between the calculated total voltage and the measured cell voltage time series by using particle swarm optimization.

4. Results

Fig. 4(a) shows the measured dynamic voltage waveforms as a function of current density and frequency. The voltage waveform is clearly observed to become more nonlinear as the frequency decreases, starting to approach the behavior of the static polarization curve.

The current density can be seen passing shortly to negative values, which indicates problems with the control of the potentiostat power supply with high amplitudes. The occurrence of negative current densities was verified to be caused by the power supply and not by errors in

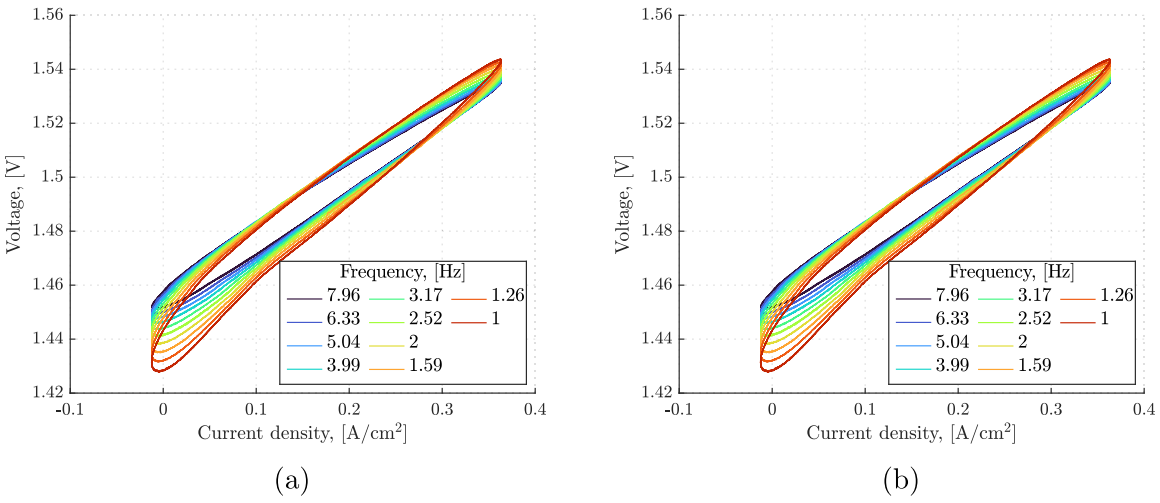

Fig. 4. (a) Measured dynamic voltage response used for model fitting and (b) the result simulated from the fitted model. Comparisons for individual frequencies are presented in Figs. A.1–A.10 of Appendix A.

the measurement system by double-checking the current measurement calibration. The power supply seemed to periodically draw current from the cell under test, mostly increasing the discharge rate of the cell capacitances. The cell voltage is still positive and above the reversible potential, which indicates that the total system can be assumed to remain in the electrolysis mode throughout the measurement.

A nonlinear response, in the form of divergence from a completely oval shape, is observed to emerge on the bottom side of the U–I curve drawn (the rising edge of the waveform) at lower frequencies, and the response is seen to start bending downwards at low current densities. A pivotal point can also be seen just below 0.1 A/cm^2, which indicates separable responses between the two electrodes of the cell. It is known from EIS measurements that the electrodes have a difference in their response times. This separation of responses can, therefore, be employed in parametrization of the two electrodes without a need for a reference electrode in the system.

The dynamic voltage response model described in Section 2.2 was fitted on the measured data, the results of which are presented in Fig. 4(b). A total of seven parameters were fitted: one for the ohmic and three for each of the activation overpotentials. The fit values for the parameters are given in Table 2. As the cathode and anode cannot be differentiated from the combined electrode response without a third electrode, the parameters may be incorrectly assigned in the fit. Therefore, a second, alternative set of parameters is added to Table 2, for which the activation overpotential parameters are flipped between the anode and the cathode, still maintaining an equivalent combined electrode performance. The basis for this parameter flipping is presented in S.1. of the supplementary material. Furthermore, the effect of the exchange current density on the voltage response at either of the electrodes is equivalent to a voltage offset [24]. As a result, the exchange current density values cannot be fixed with the presented method but can be varied according to Eqs. (S.7) and (S.8). Therefore, prior knowledge that the anode activation overpotential is generally higher than the one at the cathode, cannot be used for determining the correct order of parameters.

One noticeable aspect in the values presented in Table 2 is the electron transfer coefficient values that exceed the commonly set limits of $\alpha \in [0, 1]$. If $\alpha > 1$, the reverse reaction term in the Butler–Volmer equation (the latter exponential function in Eq. (7)) begins to have a major impact on the activation overpotential also in the forward direction. From this point of view, the values presented in Table 2 defy reason. However, according to a proof in the supplementary material of this paper, for modeling a cell as a combined electrode the electron transfer coefficient should remain between 0 and 2/3 if the single electrode electron transfer coefficients were restricted below 1. On the other hand, a fit made to the static polarization curve measurements for the given cell provided a value of $\alpha = 0.711$ (see Table 3) which could not be explained unless one or both of the single electrode electron transfer coefficients were greater than 1. This contradiction with theory puts the usage of the Butler–Volmer equation for describing the activation overpotential of water electrolyzers into questionable light. However, as the equation can reproduce the measured voltage response well, its usage for modeling purposes is justifiable. This topic is discussed further in Section 4.2.

Table 2
Parameter values obtained from the model fit and an alternative, equivalent result obtained by flipping the activation overpotential parameters for the cathode and the anode according to the proof in S.1. Error estimates for the values could not be obtained in reasonable time.

Parameter	Value		Unit
	Fit	Alternative	
r	0.191	0.191	$\Omega\,cm^2$
α_c	1.02	3.19	–
$j_{0,c}$	$2.22 \cdot 10^{-8}$	$3.63 \cdot 10^{-4}$	A/cm^2
C_c	1.45	0.200	F/cm^2
α_a	1.60	0.510	–
$j_{0,a}$	$3.63 \cdot 10^{-4}$	$2.22 \cdot 10^{-8}$	A/cm^2
C_a	0.200	1.45	F/cm^2

4.1. Model validation

The proposed model was validated by comparing its predictions with two common electrolyzer characterization measurements: the static polarization curve and the EIS. Both of the methods were simulated with the model by supplying a realistic current waveform that would be used for the respective measurement. For the static polarization curve, this means a set of defined current steps, for each of which the system is allowed to stabilize before measuring the static voltage. The EIS, on the other hand, consists of a set of small-amplitude sinusoidal ripple signals with varying frequencies that are added on top of a DC setpoint. The small amplitude allows approximating the response to be linear, which enables the calculation of a single complex impedance value for each of the frequencies. Galvanostatic EIS (GEIS) was used in this study as the model is capable of only predicting voltage response based on current input.

The simulated polarization curve is presented in Fig. 5 alongside a measured one. The model parameters of both the curves, obtained

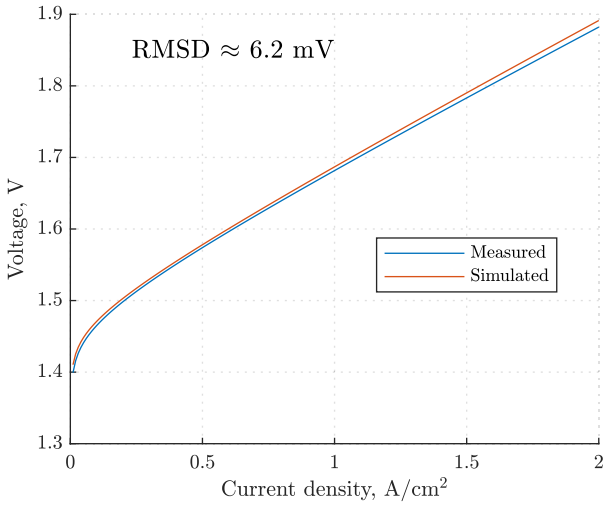

Fig. 5. Simulated polarization curve in comparison with the one measured at a different date, showing a close resemblance.

Table 3
Static polarization curve parameters fit to both the simulated and measured polarization curves. Theoretical values derived using Eqs. (S.4) and (S.5) of the supplementary material and parameters for individual electrodes from Table 2 are presented for comparison.

Parameter	Value			Unit
	Simulation	Measurement	Theoretical	
r	0.192	0.186	0.191	$\Omega\,cm^2$
α	0.779	0.711	0.772	–
j_0	$2.06 \cdot 10^{-7}$	$2.36 \cdot 10^{-7}$	$2.32 \cdot 10^{-7}$	A/cm^2

using the static fitting capability of the Electrolyzer modeling toolbox, are presented in Table 3. Hyperbolic sine approximation, Eq. (9), was used for the activation overpotential in the static fitting. Small root mean square deviation (RMSD) of approximately 6.2 mV between the simulated curve and the measured one indicates minimal difference between them.

Both qualitatively and quantitatively, the simulation matches well with the measurement. A slight divergence is observed in the ohmic resistivity, whose effect accumulates especially at high current densities. The reason for the inaccuracy might be due to the low DC setpoint used for the dynamic modeling, which minimizes the effect of the ohmic overpotential compared with the activation overpotential. Further, the polarization curve measurement was performed at a different date, which might have affected environmental parameters, such as pressure, causing a slight change in the electron transfer coefficient α.

Comparisons of the simulated and measured GEIS at the DC current density setpoint of 0.2 A/cm^2 and perturbation amplitude of 5% of the DC setpoint used for fitting the dynamic model are presented in Figs. 6(a) and 6(b). The simulation can be seen to match the measurement well, RMSD between the curves being only approximately 0.22 mΩ, yet they diverge somewhat at high frequencies.

The GEIS measurements had been performed earlier for a different study and were, therefore, in a lower temperature of 70 °C compared with the 80 °C used for the model parametrization. The temperature difference makes a meaningful quantitative comparison of the results impossible. Qualitatively, the comparison shows, however, that the presented model is well capable of simulating also voltage response at much higher frequencies than the ones used for model parametrization.

4.2. Model limitations and discussion

Although the model was capable of predicting well the dynamic voltage response, the static polarization curve, and the GEIS response

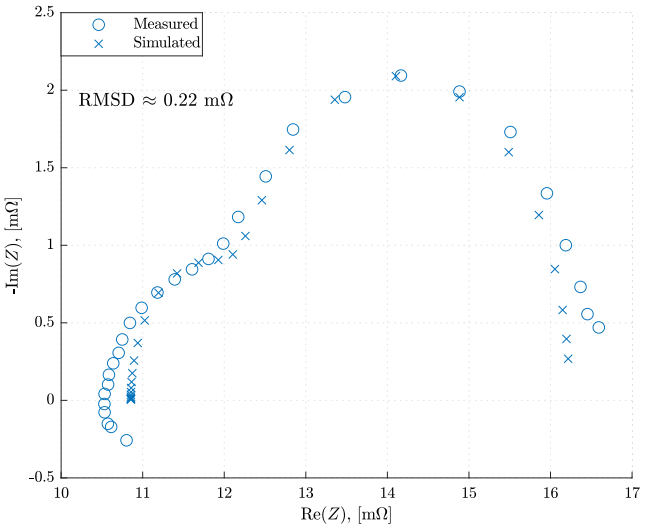

(a) Nyquist plot.

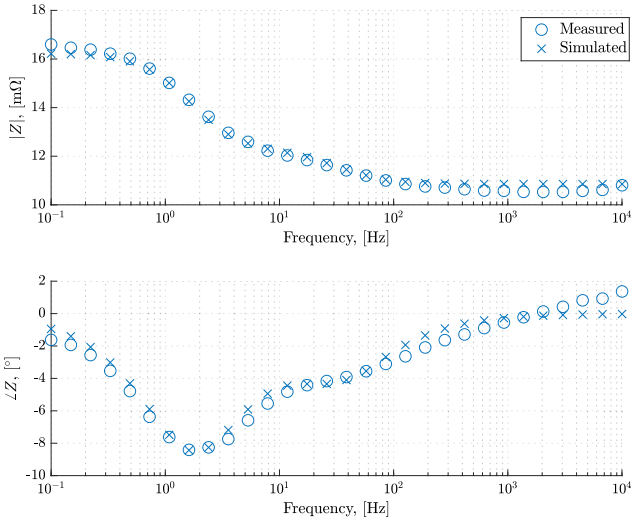

(b) Bode plot.

Fig. 6. Simulated EIS at 0.2 A/cm^2 compared with the measurement from a different date and temperature setpoint. Only the general shape of the curve should, therefore, be compared.

at the modeled DC current setpoint, some limitations of its capabilities were observed. The first limitation was noticed when the model was tested on a measurement set going down to the frequency of 0.1 Hz, presented in Fig. 7. The model was not fully capable of reproducing the behavior at the sudden change in the derivative of voltage present on the rising edge of the waveform (bottom part of the voltage–current curve). The fit results obtained from the full data set indicated that when the first one of the electrodes approaches static behavior at the lowest frequencies, its dynamic behavior diverges from what would be expected by the model. Therefore, the frequencies below 1 Hz were omitted from further analysis. Fig. 7(b) shows a comparison between the measurement and a modeled curve at 0.1 Hz with parameters obtained from the fit limited above the 1 Hz frequency. It is seen that the measured behavior is well explained by the model down to the point where the measured response has a sudden change in the derivative. This behavior could not be replicated by the model presented in this paper and would require more elaborate modeling.

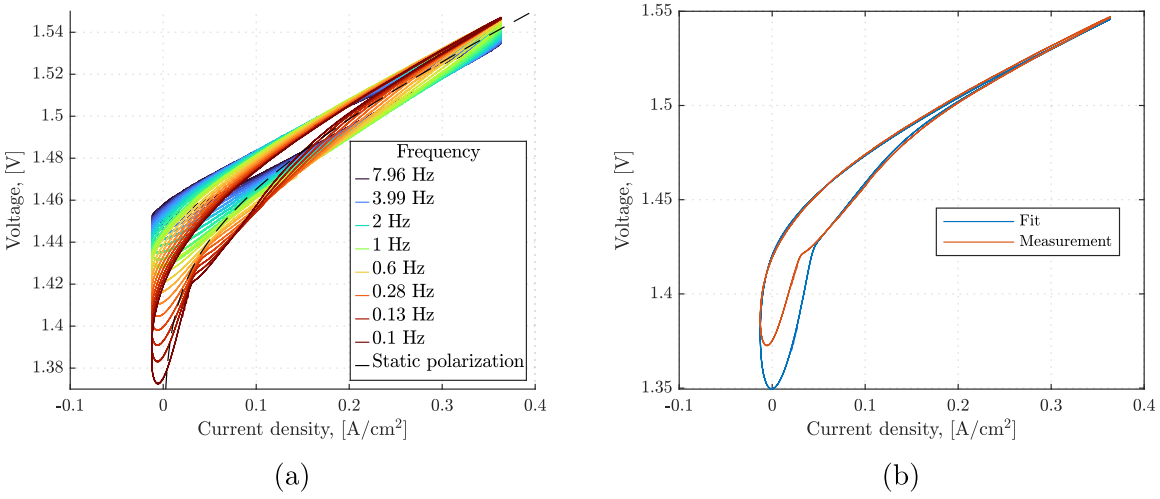

Fig. 7. (a) Full set of measured waveforms between 7.96 and 0.1 Hz and (b) comparison between the measured curve and the model prediction at 0.1 Hz.

The reasons for the reduced predictability at lower frequencies may include the voltage dependence of the capacitance [30], but also the inability of the model to simulate actual behavior when the activation overpotential at an electrode approaches zero. A further issue in such a situation may arise from the negative current densities at the lowest point of the waveform, which is filtered by the double-layer capacitance at higher frequencies but starts to have more significance at low frequencies. At worst, one of the electrodes could even reverse in polarity.

To accurately model the voltage response of a cell at lower frequencies, further three electrode measurements would be required to find out what happens on the electrodes when the frequency is reduced. Based on the proof in Sec. S.1. of the supplementary material, the exchange current density values of the electrodes cannot be fixed with a full cell model when the activation overpotential is high enough to maintain a high current density at the reaction interface. In a high-frequency dynamic setting, the double-layer capacitance smooths variations in the activation overpotential, thereby preventing the current from dropping too low. In these cases, the exchange current density affects the voltage only as an offset. This means that the value of the exchange current density on one electrode can be varied without affecting the combined voltage response, as long as the exchange current density on the other electrode is varied accordingly and neither of the electrodes approaches zero activation overpotential. The last constraint means that a full discharge of the double layer should not occur at any point of the wave, or the voltage offset behavior will break. When the frequency is lowered enough while having negative currents, one of the electrodes eventually approaches full discharge of the double layer causing the effect of the exchange current density to diverge from the mere voltage offset. This change of behavior could provide means for fixing the absolute value of the exchange current density for that electrode, fixing it also for the other electrode. Development of a methodology to take an advantage of this phenomenon would enable absolute parametrization of the model based on full cell measurements only.

The second limitation was observed from the simulated GEIS behavior in Fig. 6(a), which diverged from the measurements especially at high frequencies. One reason for this is that the model does not contain inductive components, and thus, the full high-frequency behavior cannot be taken into account. As the measurements used for fitting the model were performed at low frequencies, it is not possible to take inductive behavior at high frequencies into consideration. Separate high-frequency modeling could be performed from, e.g., the EIS measurement to obtain the necessary parameters. These could be added as a separate voltage component to the model. The scope of this paper is, however, in the low-frequency response of the cell. Thus, inclusion of high-frequency phenomena is not attempted here.

Having only two capacitive components might be an oversimplification of the reality, where diffusion might have an additional effect at low frequencies [17]. Modeling the double layers as pure capacitors might also not be accurate enough, but constant phase elements (CPE) could be required to fix the small difference observed in the phase responses at low frequencies [9]. All these changes would hinder the solvability of the modeling equations, and therefore, they were not considered in this study. Future research should concentrate on improving the methodology with more advanced models.

Further limitation of the presented model comes from the assumption of constant capacitance values. Both voltage and current dependency of the capacitances in electrochemical cells have been reported in literature [11,30,32]. Modeling the capacitance in Eq. (12) as variable would enable a wider range of applicability for the presented dynamic model. However, as the theory behind the variable capacitance is still undetailed, creating and parametrizing such a model would require more experimental research. Furthermore, all cases of variable capacitance reported in the literature are obtained from small-amplitude measurements. This might prevent observing any slowness in the change of capacitance that could influence the effect for large-amplitude signals. Because of the uncertainty in the modeling principles of variable capacitance, only constant capacitance values have been used in this paper. Further research should be conducted to consolidate the theoretical basis of variable capacitance in electrochemical cells and to investigate the possible limits on the rate of change of the capacitance values. The model parametrization principle described in this paper might prove to be useful in such studies.

One significant detail in the fit parameter values in Table 2 is that both the anode and the cathode have seemingly high electron transfer coefficient (α) values. The value of α is commonly limited to between zero and one, as otherwise the reverse reaction part of the Butler–Volmer equation, Eq. (7), having the term $(1-\alpha)$ in its exponent, would start to have an increasing effect on the current density with increasing overpotential in the forward direction. This defies reason, as the reverse reaction should diminish when the forward polarization becomes stronger. However, all the measurements performed on the cell in this study exhibit a behavior that, when modeled with the Butler–Volmer equation, could only be explained with $\alpha > 1$. Similar numbers have been presented previously in the literature by Immerz et al. [13]. Further, the combined-electrode electron transfer coefficient in static polarization curve parameters is 0.7791 according to Table 3. Based on the proof in S.1. of the supplementary material, a value this high can only be explained if one or both of the half-cell electron

transfer coefficients are greater than one. Having such a value indicates that the Butler–Volmer equation, albeit well capable of reproducing the behavior of the cell, is not exactly correct in representing the kinetics of water electrolysis. According to Noren and Hoffman [27] the Butler–Volmer equation presented in Eq. (7) is a simplification that applies to one-step, single-electron transfer processes only, which is not the case for water electrolysis. For more general modeling of multistep reactions the exact reaction mechanism and the rate determining step should be known to modify the electron transfer coefficient accordingly. When the full reaction mechanism is taken into account, electron transfer coefficient value can increase above one without causing issues with the reverse reaction. Another option would be to model the kinetics with the Tafel equation, Eq. (8), which would remove the issue with reversible reactions. However, because the large amplitude dynamics studied here can extend to very low current densities, the limited applicability range of the Tafel equation may restrict its use. Future research should, therefore, focuse on implementing the more general multistep reaction kinetics to enable obtaining physically more meaningful results from the modeling. Interested readers are encouraged to refer to the article by Noren and Hoffman [27], and Modern Electrochemistry by Bockris et al. [33] for more information on this topic.

5. Conclusion

A novel method of modeling and parametrizing water electrolyzers based on low-frequency non-linear voltage response measurements was introduced in this study. The model was built from a general polarization curve model, where the activation overpotential was replaced by a dynamic submodel. The commonly used Randles equivalent circuit was taken as the basis for the dynamic submodel, but the activation resistance was replaced by the Butler–Volmer equation, resulting in a nonlinear, nonhomogeneous differential equation. Both the anode and cathode of the cell were modeled with the same equation incorporating their unique parameters. The generated model was parametrized with a set of large-amplitude, low-frequency sinusoidal waveform measurements of current and voltage in the frequency range where the cell begins to exhibit nonlinear behavior, which is between 1 Hz and 10 Hz for the cell used in testing the model. To maximize the changes in the nonlinear response, a low DC current density setpoint of 0.2 A/cm^2 was used.

The presented model was capable of providing both parameters for half-cell Butler–Volmer equations and double-layer capacitances from measurements performed on the full cell in a small frequency range. When the half-cell Butler–Volmer equation parameters obtained from the dynamic model fit were used to calculate theoretical Butler–Volmer parameters for a static full-cell model, they agreed well with an earlier static model fit. Fixing the value for the two exchange current densities was found to be mathematically impossible as both of their influences on the full-cell voltage response are manifested as a constant voltage offset. Therefore, their values are variable within a set range without affecting the full-cell voltage response.

The proposed model was compared against a static polarization curve and qualitatively against a regular galvanostatic EIS measurement performed on the same cell but at 70 °C instead of the temperature of 80 °C used for the dynamic model fitting. The comparisons showed that the model works well for simulating the voltage response in both static and dynamic circumstances. Knowing that the dynamic response is linear at higher frequencies, depending only on the impedance [5], it can be concluded that the model is capable of simulating voltage response to arbitrary waveforms in both high and low frequency ranges regardless of the signal amplitude. This flexibility enables the model to be used for simulating the dynamic response of water electrolyzers to both varying renewable energy generation and thyristor-rectified power with ripple alike.

The model presented in this paper combines characteristics of both the static and dynamic performance of water electrolyzers. It enables parametrizing half-cell properties using full-cell measurements by taking advantage of the nonlinear voltage response at low current densities. This is an improvement to the existing characterization methods, adding dynamics to the polarization curve and expanding EIS to large amplitudes. At the same time, low-frequency high-amplitude waveform measurements performed in this study proved the actual performance of the cell to be even more complicated at the lowest frequencies, which could provide means for more thorough characterization of the system. This paper shows that clearly distinguishable half-cell phenomena can be identified and parametrized from nonlinear responses of water electrolyzers without a need for reference electrodes. Further research in this field can provide novel methodology for analyzing and monitoring the condition of water electrolyzer systems.

CRediT authorship contribution statement

Pietari Puranen: Writing – review & editing, Writing – original draft, Visualization, Validation, Software, Methodology, Investigation, Formal analysis, Data curation, Conceptualization. **Michael Hehemann:** Writing – review & editing, Validation, Resources, Methodology, Investigation. **Phillip Kütemeier:** Investigation. **Lauri Järvinen:** Writing – review & editing, Software, Methodology, Conceptualization. **Vesa Ruuskanen:** Writing – review & editing, Supervision, Resources, Project administration, Funding acquisition, Conceptualization. **Antti Kosonen:** Writing – review & editing, Supervision, Resources, Project administration, Funding acquisition, Conceptualization. **Jero Ahola:** Writing – review & editing, Supervision, Project administration, Funding acquisition, Conceptualization. **Pertti Kauranen:** Writing – review & editing, Supervision.

Declaration of competing interest

The authors declare that they have no known competing financial interests or personal relationships that could have appeared to influence the work reported in this paper.

Data availability

Data will be made available on request.

Declaration of Generative AI and AI-assisted technologies in the writing process

During the preparation of this work the authors used the GPT 3.5 large language model (ChatGPT), an AI language model by OpenAI, in order to improve the readability and clarity of some sentences written by the authors. After using this tool, the authors reviewed and edited the content as needed and take full responsibility for the content of the publication. Final language checking has been performed by a non-native professional of English linguistics.

Acknowledgments

The Academy of Finland [grant number 325791] is acknowledged for the main financial support of the Research of Power Quality Effect on Water Electrolyzer Operation (POQELYZER) project and Business Finland for the main financial support of the FinH2 (finh2.fi) project. The project partners of FinH2 are also thanked for their financial contributions. Furthermore, the Finnish Foundation for Technology Promotion and the Research Foundation of Lappeenranta University of Technology, Finland are acknowledged for their support enabling the corresponding author's research visit to the Forschungszentrum Jülich in fall 2022. Hanna Niemelä is thanked for the final language proofing of the manuscript and Andreas Glüsen for reviewing and commenting it.

Appendix A. Fit result on each of the waveforms used in the study

See Figs. A.1–A.10.

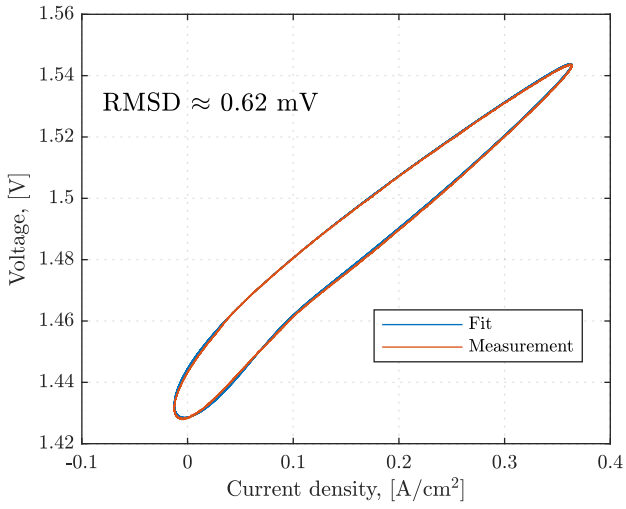

Fig. A.1. Comparison of the measured and fit voltage responses at 1 Hz.

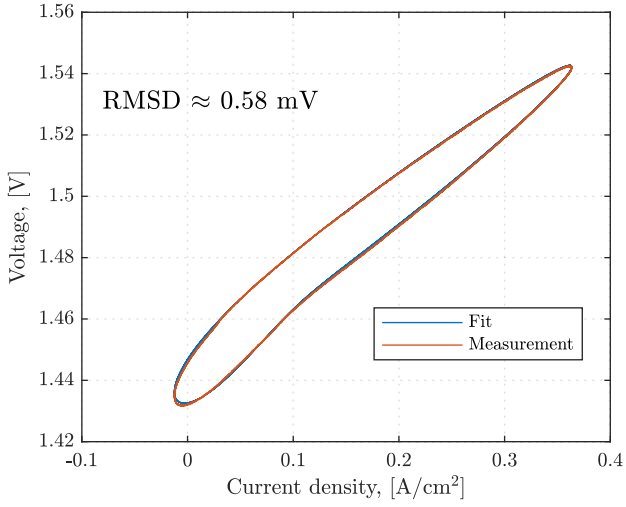

Fig. A.2. Comparison of the measured and fit voltage responses at 1.26 Hz.

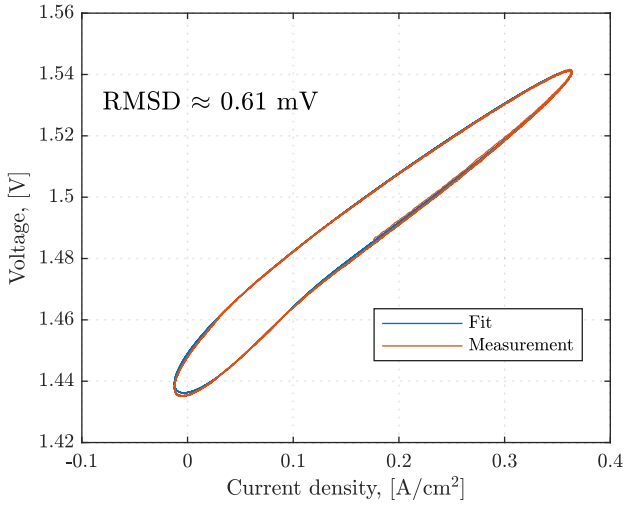

Fig. A.3. Comparison of the measured and fit voltage responses at 1.59 Hz.

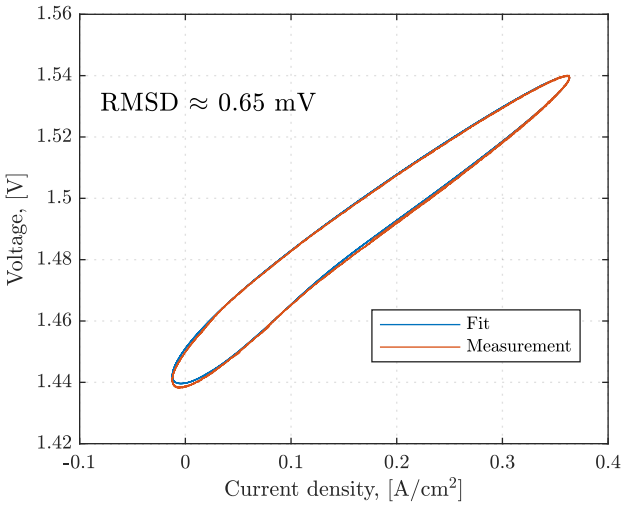

Fig. A.4. Comparison of the measured and fit voltage responses at 2 Hz.

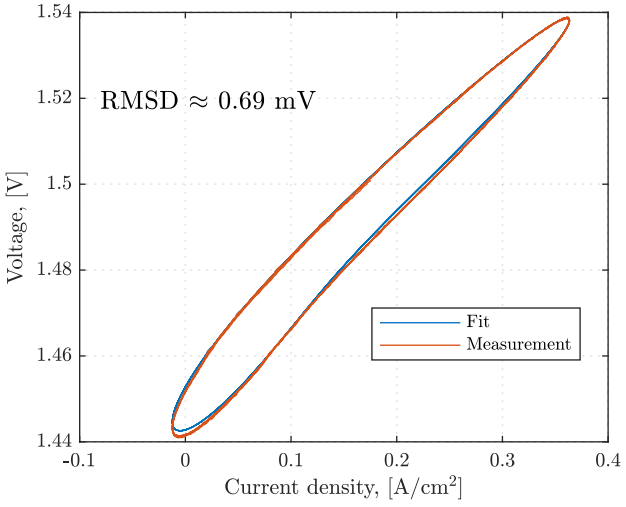

Fig. A.5. Comparison of the measured and fit voltage responses at 2.52 Hz.

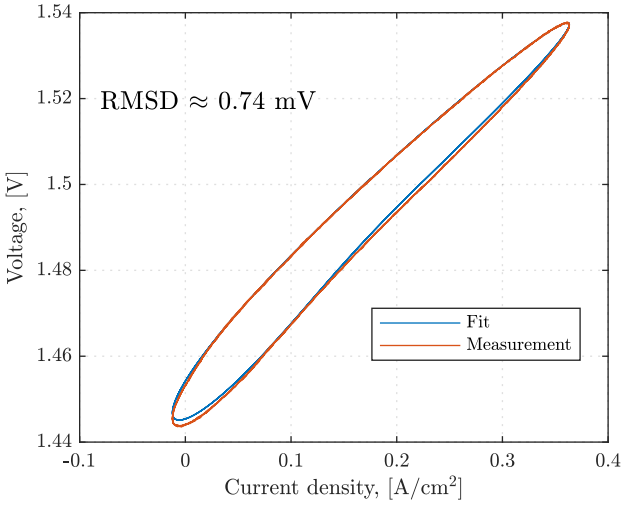

Fig. A.6. Comparison of the measured and fit voltage responses at 3.17 Hz.

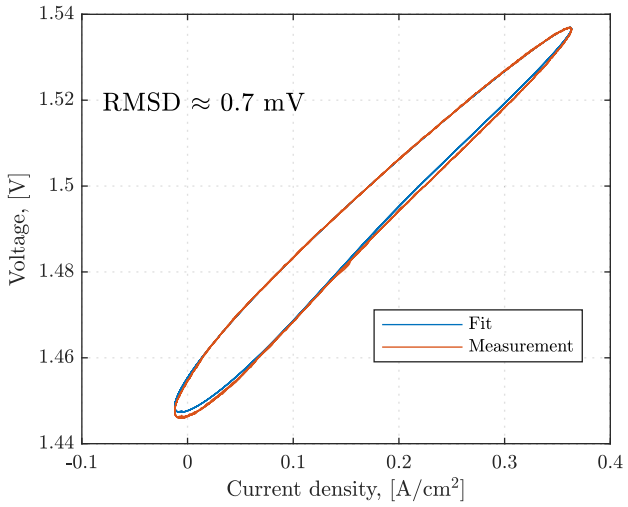

Fig. A.7. Comparison of the measured and fit voltage responses at 3.99 Hz.

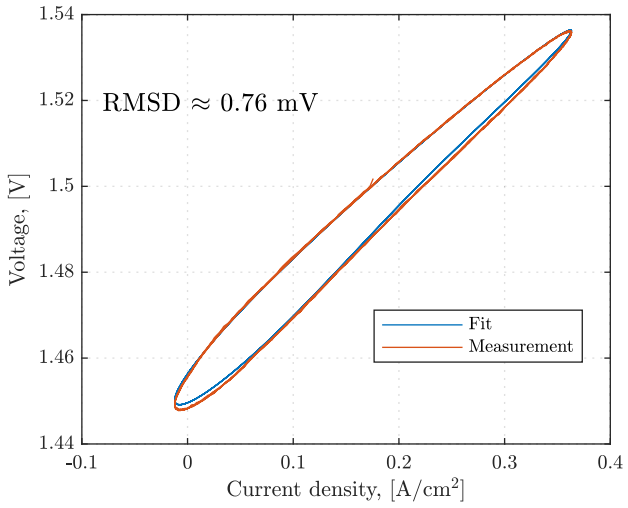

Fig. A.8. Comparison of the measured and fit voltage responses at 5.04 Hz.

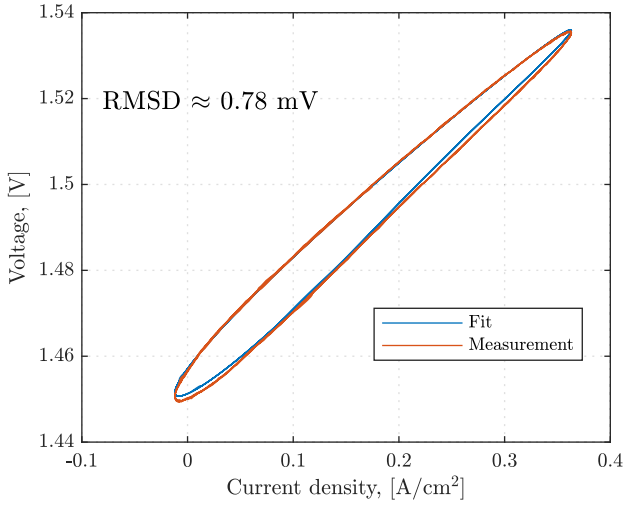

Fig. A.9. Comparison of the measured and fit voltage responses at 6.33 Hz.

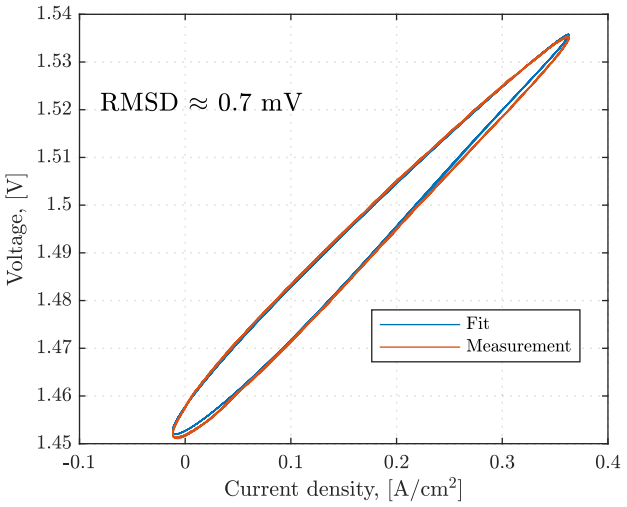

Fig. A.10. Comparison of the measured and fit voltage responses at 7.96 Hz.

Appendix B. Supplementary data

Supplementary material related to this article can be found online at https://doi.org/10.1016/j.electacta.2024.145085.

References

[1] J. Koponen, V. Ruuskanen, A. Kosonen, M. Niemelä, J. Ahola, Effect of converter topology on the specific energy consumption of alkaline water electrolyzers, IEEE Trans. Power Electron. 34 (7) (2019) 6171–6182, http://dx.doi.org/10.1109/TPEL.2018.2876636.

[2] M.R.R. Tabar, M. Anvari, G. Lohmann, D. Heinemann, M. Wächter, P. Milan, E. Lorenz, J. Peinke, Kolmogorov spectrum of renewable wind and solar power fluctuations, Eur. Phys. J. Spec. Top. 223 (12) (2014) 2637–2644, http://dx.doi.org/10.1140/epjst/e2014-02217-8.

[3] J. Koponen, V. Ruuskanen, M. Hehemann, E. Rauls, A. Kosonen, J. Ahola, D. Stolten, Effect of power quality on the design of proton exchange membrane water electrolysis systems, Appl. Energy 279 (2020) 115791, http://dx.doi.org/10.1016/j.apenergy.2020.115791.

[4] A. Lasia, The origin of the constant phase element, J. Phys. Chem. Lett. 13 (2) (2022) 580–589, http://dx.doi.org/10.1021/acs.jpclett.1c03782.

[5] P. Puranen, M. Hehemann, L. Järvinen, V. Ruuskanen, A. Kosonen, J. Ahola, P. Kauranen, Experimental study on the influence of a pem water electrolyzer cell's impedance on its power consumption under impaired power quality, 2024, http://dx.doi.org/10.2139/ssrn.4745155.

[6] D. Guilbert, G. Vitale, Experimental validation of an equivalent dynamic electrical model for a proton exchange membrane electrolyzer, in: 2018 IEEE International Conference on Environment and Electrical Engineering and 2018 IEEE Industrial and Commercial Power Systems Europe (EEEIC / I&CPS Europe), 2018, pp. 1–6, http://dx.doi.org/10.1109/EEEIC.2018.8494523.

[7] C. Martinson, G. van Schoor, K. Uren, D. Bessarabov, Equivalent electrical circuit modelling of a proton exchange membrane electrolyser based on current interruption, in: 2013 IEEE International Conference on Industrial Technology (ICIT), 2013, pp. 716–721, http://dx.doi.org/10.1109/ICIT.2013.6505760.

[8] P.J.H. Wingelaar, J.L. Duarte, M.A.M. Hendrix, PEM fuel cell model representing steady-state, small-signal and large-signal characteristics, J. Power Sources 171 (2) (2007) 754–762, http://dx.doi.org/10.1016/j.jpowsour.2007.06.001.

[9] O. Sologubenko, R. Castiglioni, S. Pettersson, A.A. Leal, D. Chartouni, F. Canales, Dynamic impedance modeling of an alkaline electrolyzer – A practical approach, in: 2023 International Workshop on Impedance Spectroscopy (IWIS), 2023, pp. 109–114, http://dx.doi.org/10.1109/IWIS61214.2023.10302772.

[10] S.F. Amireh, N.N. Heineman, P. Vermeulen, R.L.G. Barros, D. Yang, J. van der Schaaf, M.T. de Groot, Impact of power supply fluctuation and part load operation on the efficiency of alkaline water electrolysis, J. Power Sources 560 (2023) 232629, http://dx.doi.org/10.1016/j.jpowsour.2023.232629.

[11] A. Ursúa, P. Sanchis, Static-dynamic modelling of the electrical behaviour of a commercial advanced alkaline water electrolyser, Int. J. Hydrog. Energy 37 (24) (2012) 18598–18614, http://dx.doi.org/10.1016/j.ijhydene.2012.09.125.

[12] F. Zenith, F. Seland, O.E. Kongstein, B. Børresen, R. Tunold, S. Skogestad, Control-oriented modelling and experimental study of the transient response of a high-temperature polymer fuel cell, J. Power Sources 162 (1) (2006) 215–227, http://dx.doi.org/10.1016/j.jpowsour.2006.06.022.

[13] C. Immerz, B. Bensmann, P. Trinke, M. Suermann, R. Hanke-Rauschenbach, Understanding electrical under- and overshoots in proton exchange membrane water electrolysis cells, J. Electrochem. Soc. 166 (15) (2019) F1200, http://dx.doi.org/10.1149/2.0881914jes.

[14] T. Krenz, T. Gottschalk, L. Helmers, P. Trinke, B. Bensmann, R. Hanke-Rauschenbach, Current interrupt technique to fully characterize PEMWE cells, J. Electrochem. Soc. 171 (3) (2024) 034509, http://dx.doi.org/10.1149/1945-7111/ad3057.

[15] F. Fasmin, R. Srinivasan, Review—nonlinear electrochemical impedance spectroscopy, J. Electrochem. Soc. 164 (7) (2017) H443, http://dx.doi.org/10.1149/2.0391707jes.

[16] T. Vidaković-Koch, T. Miličić, L.A. Živković, H.S. Chan, U. Krewer, M. Petkovska, Nonlinear frequency response analysis: A recent review and perspectives, Curr. Opin. Electrochem. 30 (2021) 100851, http://dx.doi.org/10.1016/j.coelec.2021.100851.

[17] N. Wolff, N. Harting, F. Röder, M. Heinrich, U. Krewer, Understanding nonlinearity in electrochemical systems, Eur. Phys. J. Spec. Top. 227 (18) (2019) 2617–2640, http://dx.doi.org/10.1140/epjst/e2019-800135-2.

[18] Q. Mao, U. Krewer, Total harmonic distortion analysis of oxygen reduction reaction in proton exchange membrane fuel cells, Electrochim. Acta 103 (2013) 188–198, http://dx.doi.org/10.1016/j.electacta.2013.03.194.

[19] T. Kadyk, R. Hanke-Rauschenbach, K. Sundmacher, Nonlinear frequency response analysis for the diagnosis of carbon monoxide poisoning in PEM fuel cell anodes, J. Appl. Electrochem. 41 (9) (2011) 1021–1032, http://dx.doi.org/10.1007/s10800-011-0298-8.

[20] B. Bensmann, M. Petkovska, T. Vidaković-Koch, R. Hanke-Rauschenbach, K. Sundmacher, Nonlinear frequency response of electrochemical methanol oxidation kinetics: A theoretical analysis, J. Electrochem. Soc. 157 (9) (2010) B1279, http://dx.doi.org/10.1149/1.3446836.

[21] N. Wolff, N. Harting, M. Heinrich, U. Krewer, Nonlinear frequency response analysis on lithium-ion batteries: Process identification and differences between transient and steady-state behavior, Electrochim. Acta 298 (2019) 788–798, http://dx.doi.org/10.1016/j.electacta.2018.12.107.

[22] N. Harting, N. Wolff, F. Röder, U. Krewer, Nonlinear frequency response analysis (NFRA) of lithium-ion batteries, Electrochim. Acta 248 (2017) 133–139, http://dx.doi.org/10.1016/j.electacta.2017.04.037.

[23] L. Järvinen, P. Puranen, Electrolyzer modelling toolbox, 2023, https://se.mathworks.com/matlabcentral/fileexchange/117175-electrolyzer-modelling-toolbox. (Accessed 27 March 2023).

[24] L. Järvinen, P. Puranen, A. Kosonen, V. Ruuskanen, J. Ahola, P. Kauranen, M. Hehemann, Automized parametrization of PEM and alkaline water electrolyzer polarisation curves, Int. J. Hydrog. Energy 47 (75) (2022) 31985–32003, http://dx.doi.org/10.1016/j.ijhydene.2022.07.085.

[25] M. Schalenbach, Proton Conduction and Gas Permeation through Polymer Electrolyte Membranes during Water Electrolysis (Ph.D. thesis), RWTH Aachen University, Forschungszentrum Jülich GmbH, 2018.

[26] J. Balej, Water vapour partial pressures and water activities in potassium and sodium hydroxide solutions over wide concentration and temperature ranges, Int. J. Hydrog. Energy 10 (4) (1985) 233–243.

[27] D.A. Noren, M.A. Hoffman, Clarifying the Butler–Volmer equation and related approximations for calculating activation losses in solid oxide fuel cell models, J. Power Sources 152 (2005) 175–181, http://dx.doi.org/10.1016/j.jpowsour.2005.03.174.

[28] T. Smolinka, E.T. Ojong, T. Lickert, Fundamentals of PEM water electrolysis, in: D. Bessarabov, H. Wang, H. Li, N. Zhao (Eds.), PEM Electrolysis for Hydrogen Production: Principles and Applications, CRC Press, 2016, pp. 11–33.

[29] S.W. Boettcher, S.Z. Oener, M.C. Lonergan, Y. Surendranath, S. Ardo, C. Brozek, P.A. Kempler, Potentially confusing: potentials in electrochemistry, ACS Energy Lett. 6 (1) (2021) 261–266, http://dx.doi.org/10.1021/acsenergylett.0c02443.

[30] M. Schalenbach, Y. Emre Durmus, H. Tempel, H. Kungl, R.-A. Eichel, Double layer capacitances analysed with impedance spectroscopy and cyclic voltammetry: Validity and limits of the constant phase element parameterization, Phys. Chem. Chem. Phys. 23 (37) (2021) 21097–21105, http://dx.doi.org/10.1039/D1CP03381F.

[31] MathWorks Inc, Ode89 documentation, 2024, https://se.mathworks.com/help/matlab/ref/ode89.html. (Accessed 13 March 2024).

[32] M. He, G. Nie, H. Yang, B. Li, S. Zhou, X. Wang, X. Meng, A generic equivalent circuit model for PEM electrolyzer with multi-timescale and stages under multi-mode control, Appl. Energy 359 (2024) 122728, http://dx.doi.org/10.1016/j.apenergy.2024.122728.

[33] J.O. Bockris, A.K.N. Reddy, M. Gamboa-Aldeco, second ed., Modern Electrochemistry, vol. 2A: Fundamentals of Electrodics, Kluwer Academic Publishiers, 2002.